Automated Front Wall Feature Extraction and Material Assessment Using Fused LIDAR and Through-Wall Radar Imagery

Pascale Sévigny and Jonathan Fournier
Defence Research and Development Canada (DRDC)
CANADA

Pascale.Sevigny@drdc-rddc.gc.ca
Jonathan.Fournier@drdc-rddc.gc.ca

ABSTRACT

Military forces operating in urban environments are facing numerous challenges. One of them consists in being able to identify buildings material to support missions involving tactical breach or blast damage prediction. This paper reports on a method that combines both LIDAR and through-wall radar imagery to provide detailed information about a building front wall features and its construction material. The LIDAR and 3-D through-wall synthetic aperture radar (TWSAR) are mounted on a vehicle which is driven in front of a building/wall of interest. The acquired LIDAR point cloud is post-processed to automatically extract information on the front wall of buildings using a plane search strategy and cluster extraction to generate a front wall occupancy grid. This occupancy grid is used by the through-wall radar processing algorithms to restrict imagery to the areas of the wall that are exempt of doors, windows, or any other external feature. Based on typical features found in the through-wall radar images of the front wall, the type of wall is categorized as vinyl/gypsum/wood studs, cinder block, brick and cinder block, poured concrete, or others. The combination of LIDAR and through-wall radar offers the unique opportunity to automate the front wall feature extraction and material assessment and to provide timely information to a potential user.

1.0 INTRODUCTION

Military forces operating in urban environments are facing numerous challenges. One of them consists in being able to identify buildings material to support missions involving tactical breach or blast damage prediction. The exterior layer of a building can typically be identified by visual inspection or with the aid of cameras [1]. The use of a LIDAR (LIght Detection And Ranging) further provides high-resolution information about external features on the exterior wall, such as 3-D location of doors and windows and of any object such as rain gutters, pipes, etc [2][3].

Some military missions would benefit from additional knowledge about a building's wall, for example its thickness, its composition, and the presence of any object or perpendicular wall directly against it. The use of radars is acknowledged as a non-intrusive method for assessing wall materials and has been used in the context of historic buildings restoration [4] and civil engineering [5]. The use of radars for military purposes imposes the additional requirement of remote and possibly covert operations.

This paper reports on a method that combines both LIDAR and through-wall radar imagery to provide detailed information about a building front wall features and its construction material. The LIDAR and 3-D through-wall synthetic aperture radar (TWSAR) are mounted on a vehicle which is driven in front of a building/wall of interest while collecting data. One pass in front of a wall is sufficient to gather the wall data for further post-processing. Details of the experimental data acquisitions can be found in Section 2.

The acquired LIDAR point cloud is post-processed to automatically extract information on the front wall of buildings using a plane search strategy and cluster extraction to generate a front wall occupancy grid. This occupancy grid is used to feed the through-wall radar algorithms with the coordinates of openings (doors, windows) and portions of the front wall that are not covered by external features. The LIDAR data processing is described in Section 3.

3-D through-wall radar imagery is produced of the front wall and of its radar signature. The signature is characterized by radar signal reflections at interfaces between different layers of a wall, for example air-wall or brick-cinder block interfaces. The signature also includes multipath propagation signals between the different layers or created by air gaps, such as those found within cinder blocks. The through-wall radar signature, due to the multipath signals, typically extends in range beyond the actual physical depth of the wall. A method, based on typical features found in the through-wall radar images of the front wall, is presented which automatically categorizes the type of wall material (amongst vinyl/gypsum/wood studs, cinder block, brick and cinder block, poured concrete, others). Once a wall is categorized, post-processing algorithms specific to each category can provide additional information on the wall. The TWSAR data processing and experimental results are presented in Section 4.

Finally, a conclusion is provided in Section 5.

2.0 VEHICLE-BASED LIDAR AND TWSAR SYSTEMS

The vehicle shown in Figure 1 is equipped with the DRDC TWSAR system and its antennas mounted on the side, and the LIDAR mounted on the rooftop. The LIDAR sensor is a line-scanning Riegl VZ400. It was set to scan 120 lines per second in the vertical direction. Using motion of the vehicle in the horizontal direction and geo-positioning data, the LIDAR provides point clouds of the exterior of buildings in 3-D. The geo-positioning system used for this project is the Applanix POS-LV 420.

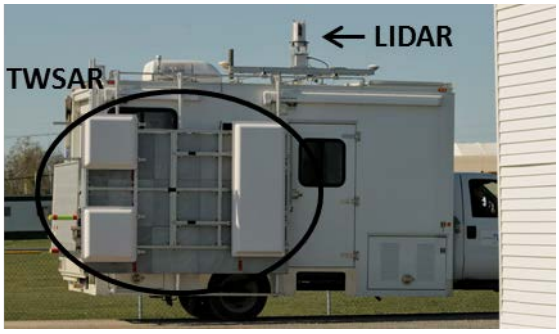

Figure 1: Vehicle with the TWSAR antennas mounted on its side and the LIDAR on its rooftop.

The TWSAR system is a linear frequency modulation ultra-wideband radar operating from 0.8 to 2.7 GHz, providing approximately 12 cm of range resolution. Vertical polarization is used. It has an eight-element linear vertical array and two transmit antennas that are toggled in time. It is thus operated as a slow-time multiple input multiple-output (MIMO) radar for doubled resolution in the elevation direction.

The LIDAR and TWSAR systems are both time-synchronized with the geo-positioning system. They share a common frame of reference and the aligned data outputs can be fused.

2.1 Data acquisitions

Experimental data was collected of 17 different walls. Four main categories are defined, and a fifth one consists of other unusual walls for which we do not have enough samples to make a distinct category (one simple wood wall (w1), one metallic sea container wall (m1), one brick wall (b1) and one cinder block wall coated with a layer of cement of unknown thickness (u1)). Among each category, minor variations between walls can be found. For example, regular and split-face cinder blocks are in the same category and assigned wall numbers c1 to c5. Brick plus cinder block walls are grouped whether the cinder blocks are 4 or 6 inches deep; they are assigned wall numbers bc1 and bc2. The gypsum/wood stud walls can have various coatings; they are assigned wall numbers s1 to s3. The poured concrete walls can have different thicknesses; they are assigned wall numbers p1 to p3.

3.0 LIDAR DATA PROCESSING

The 3D point cloud of a building's facade is generated by combining the LIDAR data collected with the Rigel VZ400 laser scanner and the trajectory of the vehicle recorded with the Applanix POS-LV geo-positioning system. This point cloud captures the external features of the building and can be used to complement the processing of the TWSAR data. For example, the point cloud of a vinyl/gypsum/wood studs wall building is shown in Figure 2b along with a photograph in Figure 2a.

For a given 3-D point cloud containing one or several buildings of interest, the objectives of the point cloud processing are:

1. To automatically find wall planes in the collected point cloud; and
2. To generate a 2D occupancy grid of the wall that indicates which parts of the wall are solid and which parts are obstructed by foreground objects or correspond to openings in the wall.

3.1 Extraction of wall planes

In order to find wall and ground points in the point cloud, a plane search algorithm is used. This algorithm relies on an optimized version of the Random sample consensus (RANSAC) algorithm [6]. With the improved version of the algorithm, a point is considered to be part of a plane if it meets two criteria: 1) its distance to the plane must be below a given threshold and 2) its corresponding local normal vector must be aligned with the normal of the plane.

The first step of the processing consists in removing the ground points from the point cloud. Using the plane search algorithm, the planes with a normal which has a strong vertical component are iteratively removed from the point cloud. Once ground points have been removed, the point cloud is cleaned from the remaining outliers. Outliers are defined as points with less than five neighbours within a 0.2 m radius.

The remaining points are then grouped into clusters using a method called Euclidean Cluster Extraction [7]. The minimum number of points in a cluster is set to 10 and the maximum distance between two points that are part of the same cluster is set to 0.5 m. The extracted clusters for the example building are shown in Figure 2c. Four clusters are extracted: the front wall, two fences on each side of the building, the utility pole and cables, the hill behind and to the side of the building.

Potential wall planes are found by analyzing each cluster using the plane search algorithm described above. Planes are defined as potential walls if they are vertical and their normal is perpendicular to the direction of travel of the vehicle. Potential wall planes are considered to be real walls if their height is greater than 1.7 m (5 ft) and their area is greater than $2m^2$. For the example building, one cluster is determined to be a real wall (Figure 2d).

3.2 Occupancy grid generation

The occupancy grid is an array of discrete cells which gives information on the different parts of the wall. It is generated by projecting the 3-D points that are collected over the volume defined by the wall on the 2-D plane that corresponds to the wall.

There are four possible states that can be assigned to a cell: *solid wall, non-solid wall, transparent* and *undefined*. The *solid wall* state is assigned to cells which represent the wall material. Objects located in front of the walls (e.g. electrical boxes, poles) fall in the *non-solid wall* category while openings with transparent material (such as windows) are marked as *transparent*. The *undefined* state is assigned to cell representing areas where no 3-D points were collected on the wall and generally correspond to obstructed windows, doors and other openings.

By clustering the occupancy cells together, it is possible to generate an occupancy map $M_w(x,z)$ of the wall (Figure 2e) which can be used during the processing of the TWSAR data. In particular, the TWSAR data processing requires information on the x values for which 75% of the occupancy grid are of the solid wall state, defined here as the set x_w:

$$x_i \in x_w \text{ if } 75\% \text{ of } M_w(x_i,z)|_{\text{all } z} \text{ is solid wall}$$

$$x_i \notin x_w \text{ otherwise}$$

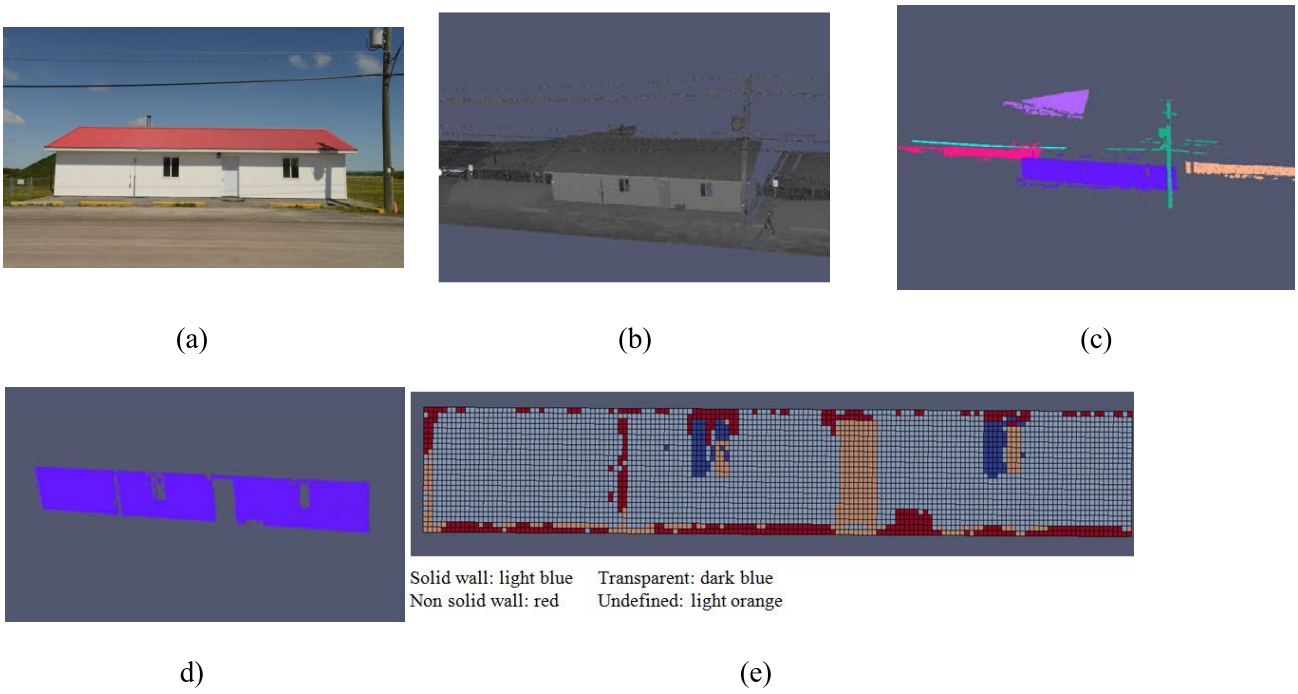

(a) (b) (c)

d) (e)

Figure 2: (a) Photograph. (b) LIDAR point cloud. (c) Extracted clusters. (d) Wall plane point cloud. (e) Occupancy grid.

4.0 TWSAR DATA PROCESSING

4.1 Image formation

For each data acquisition, two 3-D SAR images are processed using a time-domain backprojection algorithm [8]. The total number of transmit locations contributing to the coherent integration is restricted to keep a fixed synthetic aperture angle, and therefore an equal azimuth resolution, at all ranges. For this study, two synthetic aperture angles were used, of 50 and 90 degrees, resulting in two 3-D SAR images that are denoted here as $I^{50}(x,y,z)$ and $I^{90}(x,y,z)$, respectively, where x,y,z refer to the azimuth, range and elevation directions. The intensity (power) of the SAR images on a logarithmic scale (in decibels) is considered in this study.

The 50 degree synthetic aperture angle is the default angle used for TWSAR image formation, while the 90 degree synthetic aperture angle highlights signal contributions from corners. The latter is particularly useful for inhomogeneous walls with inside corners formed by air gaps inside cinder blocks or between wood studs. For the purpose of wall assessment, the 3-D SAR images are formed on a grid with very fine spacing (on the order of a sixth of the radar resolution), extending over the entire building in the x or azimuth or along-track direction,

and extending 1.5 m behind the exterior interface of the wall (in the y or range direction). The wall radar signature is the superposition of signals reflected at all the interfaces between layers of the wall, as well as multi-path propagation between the different layers, and can thus be visible over a range much larger than the actual thickness of the wall. For each 3-D SAR image, the elevation slice for which the wall signal is strongest ($z = z_w$) is determined automatically. This elevation typically corresponds to the elevation of the antenna phase centre. In what follows, only the 2-D slices at that elevation are considered for further processing. The processing is also restricted to the azimuth boundaries provided by the LIDAR post-processing algorithm defined above as x_w, consisting of areas of the wall not covered by any external feature or occupied by doors or windows.

In Figure 3 are eight exemplars of 2-D SAR images from different wall materials, which show very different signatures. On these images, the radar path is at the bottom (from right to left) and at a standoff distance of 5 to 15 m from the wall. The first yellow line at the bottom of the images corresponds to the air-wall exterior interface and is typically fairly smooth over the x axis. The strength of that line depends on the material dielectric constant but is unfortunately not a direct measure of it. A second line can be defined for all walls. It can be relatively weak or strong, smooth or uneven, depending on the homogeneity of the wall. It can be due to the second interface found in the wall, such as between bricks and cinder blocks, or it can be the result of a superposition of signals from a few interfaces when these are thinner than the limited radar resolution.

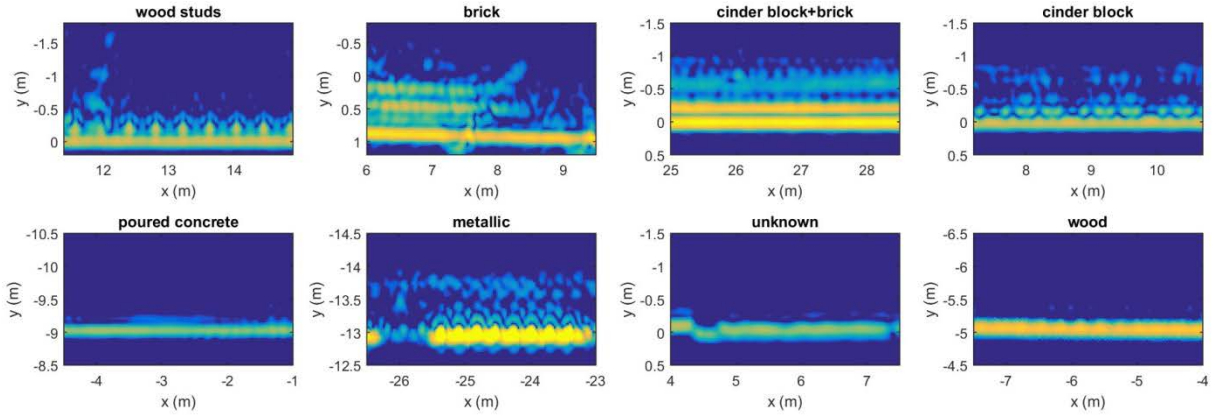

Figure 3: 2-D top view slices of 3-D SAR images processed with a 90 degree synthetic aperture angle, at the height of the maximum wall signature strength, for eight different walls. The images are normalized and shown on the same scale of 0 to 25 dB.

4.2 Feature extraction and wall category prediction

The 2-D SAR images at $z = z_w$, restricted to $x \in x_w$, are the input to the wall feature extraction, i.e. $I^{50}(x \in x_w, y, z_w)$ and $I^{90}(x \in x_w, y, z_w)$. The mean and standard deviation over all x_w values are computed, for each range value. This results in a mean range profile and a standard deviation range profile, as follows for the 50 degree synthetic aperture angle case:

$$m^{50}(y) = \frac{1}{N_{x_w}} \sum_{x \in x_w} I^{50}(x, y, z_w)$$

$$s^{50}(y) = \sqrt{\frac{1}{N_{x_w}-1} \sum_{x \in x_w} \left(I^{50}(x, y, z_w) - m^{50}(y)\right)^2}$$

N_{x_w} is the number of discretized x_w values. The definitions for $m^{90}(y)$ and $s^{90}(y)$ are equivalent. Comparing the four range profiles, the two range bins of the two strongest peaks are determined, corresponding to the first and second lines described above, and denoted as y_{FL} and y_{SL}. The mean and standard deviation for these two range bins and for the 50 and 90 degree cases are kept for further processing, as well as the averaged 50 and 90 degree values. They are defined as

$$\{m_{FL}^{50} = m^{50}(y_{FL}), m_{FL}^{90} = m^{90}(y_{FL}), m_{FL} = (m_{FL}^{50} + m_{FL}^{90})/2, \},$$

for the mean range profile case. The complete set of values of interest is as follows:

$$\{m_{FL}^{50}, m_{FL}^{90}, m_{FL}, m_{SL}^{50}, m_{SL}^{90}, m_{SL}, s_{FL}^{50}, s_{FL}^{90}, s_{FL}, s_{SL}^{50}, s_{SL}^{90}, s_{SL}\}.$$

The following observations can be made based on the values defined above, leading to four features.

- In the case of the brick+cinder block walls, the first two lines are almost equally strong. Feature 1 is defined as the difference between the mean values of these two lines:

  $$\text{Feature 1} = m_{FL} - m_{SL}$$

  Feature 1 is less than 3 dB for the brick+cinder block wall category. It is larger than 3 dB for all the other walls assessed. For the metallic and wood walls, the second line is the result of sidelobes in the radar point spread function. This is because the radar signal does not penetrate the metallic wall, and the wood wall is thinner than the radar range resolution and the reflected signals at the two interfaces are merged into one line. As a result, Feature 1 is very large for these two walls, more than 19 dB.

- For very inhomogeneous walls such as the vinyl/gypsum/wood stud walls, the standard deviation of the second line is larger than the standard deviation at the first line. Feature 2 is defined as the difference between the standard deviation at the two lines:

  $$\text{Feature 2} = s_{FL} - s_{SL}$$

  Feature 2 is negative for the vinyl/gypsum/wood stud walls. It turns out to be relatively small for the brick+cinder block walls, since the two lines are almost equally strong and smooth. For the poured concrete walls, the second line is very weak and hence its standard deviation, while the first line is strong and shows a corresponding larger standard deviation. Feature 2 is large. The same happens for the cinder block walls, even though the second line is quite uneven but is quite weak. Feature 2 is even larger for the metallic and wood walls, due to the quasi-absence of the second line, as discussed above.

- The difference between the mean and standard deviation for the first line is always relatively large (2 to 10 dB). When the wall is very inhomogeneous (cinder block or vinyl/gypsum/wood stud walls) then the difference between the mean and standard deviation for the second line is relatively small in comparison. Feature 3 captures this observation:

  $$\text{Feature 3} = \frac{|(m_{FL} - s_{FL}) - (m_{SL} - s_{SL})|}{(m_{FL} - s_{FL})}$$

- The difference between the 50 and 90 degree range profiles are more apparent for the second line. Feature 4 captures the difference between the mean and standard deviation values for the 50 and 90 degree processing, for the second line only. The poured concrete walls are the only ones with a relatively large value for this feature.

  $$\text{Feature 4} = |(m_{SL}^{50} - s_{SL}^{50}) - (m_{SL}^{90} - s_{SL}^{90})|$$

In Figure 4 is plotted the values for Feature 2 versus Feature 3, for all walls considered in this study. These two features are almost sufficient to categorize most walls. The two walls that are brick+cinder block (bc1 and bc2) are closely grouped far from the other walls. They are the easiest to distinguish. The use of Feature 1 would simply re-inforce this finding. The m1 and w1 walls are outliers with a large value for feature 2. The vinyl/gypsum/wood stud walls (s1 to s3) are also closely grouped and easy to distinguish. The cinder block walls (c1 to c5) are grouped into one cluster, except for one wall (c2) which is closer to the cluster of the poured concrete walls (p1 to p3). The brick wall (b1) appears categorized as a cinder block wall. When looking at the SAR images, it seems that considering features of the third line would be required to separate the brick wall from the cinder block walls. We do not have a sufficient number of samples from this type of wall to do better at this time. The unknown wall (u1) is made of cinder blocks covered by a layer of cement of unknown thickness. It appears to be clustered with the poured concrete walls, which seems realistic at this point.

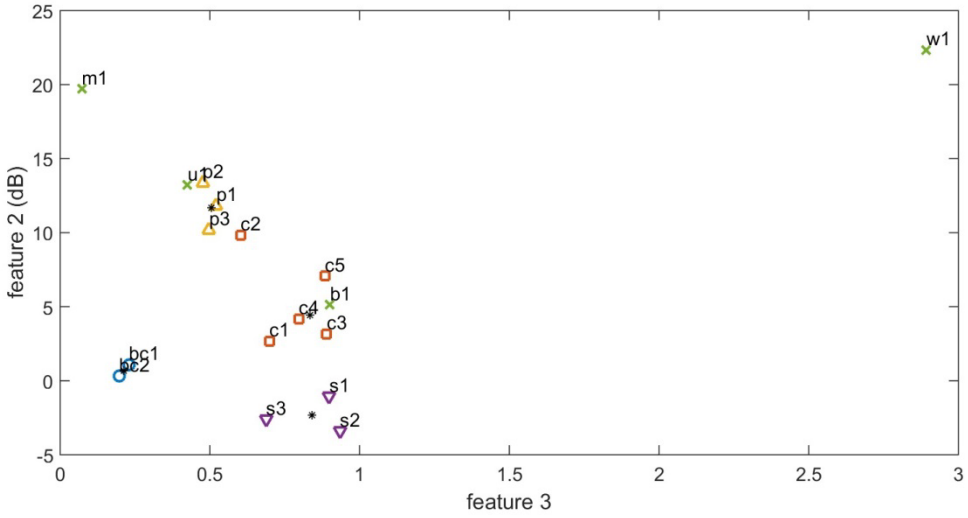

Figure 4: Feature 2 versus Feature 3, for all walls tested.

On Figure 4 are overlaid as black stars the results of clustering the normalized values of Features 2 and 3 in four categories, for all walls except m1 and w1. Using these cluster centroids and ignoring the walls with a feature 2 value greater than 19 dB (the m1 and w1 outlier walls), all remaining walls are correctly predicted except for one cinder block wall (c2) which is predicted as a poured concrete wall.

The results of clustering using all four features are not as satisfying (results not shown). These features are to be retained for use in a supervised classifier approach using Support Vector Machines (SVMs) for example, where more features are desirable and softer boundaries between classes are acceptable. We do not have sufficient samples at this time for proper training and cross-validation of such a classifier. Instead we will use Features 2 and 3 only for wall categorization.

4.3. Thickness and dielectric constant estimates

Once a wall is classified into a given category, additional information can be extracted using category-specific processing. In principle, one could use the distance between the first two lines $d_{app} = y_{SL} - y_{FL}$ to estimate the dielectric constant given prior knowledge of typical thicknesses in building materials, given that

$$d = \frac{|y_{SL} - y_{FL}|}{\sqrt{\epsilon_r}},$$

where d is the actual thickness of a layer and ϵ is the relative dielectric permittivity or dielectric constant of the material. In reality and given the limited resolution of the radar, these estimates should be obtained using a model of the wall taking into account the superposition of reflected signals at interfaces of all layers as well as some multi-path signals. This is beyond the scope of this paper.

4.4 Behind the wall information extraction

Some of the wall radar signatures show a very distinct and periodic pattern. For the case of the vinyl/gypsum/wood stud walls, this can be used to detect anomalies behind the wall, such as the presence of furniture or an internal wall perpendicular to the wall being assessed. In Figure 5 is shown the top view SAR image of one such wall for the building of Figure 2**.** It is 15 m long and has two windows, one door and one exterior vertical metallic pipe on the front wall. The SAR image is annotated with the features of interest. To detect anomalies behind that wall, we used one section of the wall as a reference (centred on $x = 13.42$ m). The section is 40 cm wide in the x direction (corresponding to one period due to the 16 inches wood stud spacing) and includes all range bins. It is denoted as $P(x_i, y_j)$, where x_i and y_j refer to the discretized x and y values, respectively. We use the sum of absolute differences (SAD) as a measure of the similarity between the reference section and all sections of the wall. The SAD is defined as

$$SAD(x_i) = \sum_{k=0}^{N_x-1} \sum_{k'=0}^{N_y-1} |I^{50}(x_i + k, k', z_w) - P(k, k')|,$$

where N_x and N_y are the number of discrete x and y values. A low SAD corresponds to a good match. Given the periodicity of the wall signature, we expect the SAD to show a similar periodic pattern. The SAD is plotted in Figure 5. We overlay as rectangular windows the values provided by the LIDAR identifying sections of the wall that are free of external features (i.e., $x \in x_w$). The SAD values are higher at the location of the indoor electric panel and the internal wall, indicating the locations of possible anomalies behind the wall (red arrows).

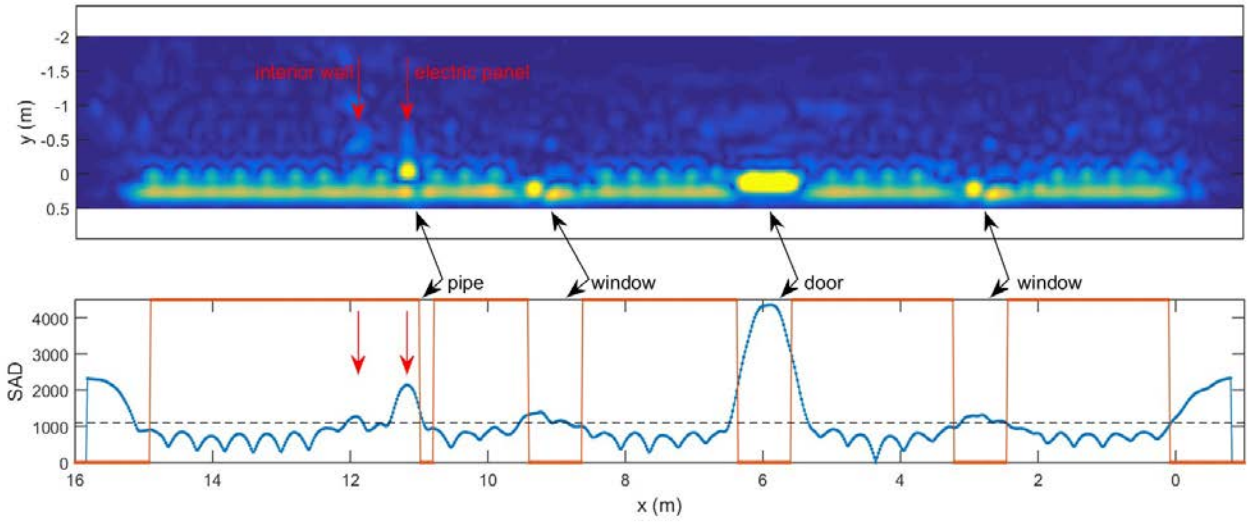

Figure 5: Top view SAR image of a vinyl/gypsum/wood stud wall and the corresponding Sum of Absolute Differences (SAD).

5.0 CONCLUSION

In this paper is presented a method using fusion of LIDAR and through-wall radar information to extract wall features and assess wall material. The LIDAR and through-wall radar data processing algorithms are described. The results of the categorization of 17 different walls (amongst vinyl/gypsum/wood studs, cinder block, brick and cinder block, poured concrete, or others) are reported. Additional data processing algorithms are suggested to infer the presence of anomalies behind walls. More experimental data sets of an even greater variety of walls will be required to improve and validate the preliminary results presented in this paper. Nonetheless, it is demonstrated that the combination of LIDAR and through-wall radar offers the unique opportunity to automate the front wall feature extraction and material assessment with the goal to provide timely information to a potential user.

6.0 REFERENCES

[1] Hoegner, L., & Stilla, U. (2009). Thermal leakage detection on building facades using infrared textures generated by mobile mapping. *2009 Joint Urban Remote Sensing Event*, 1-6.

[2] Pu, S., & Vosselman, G. (2009). Knowledge based reconstruction of building models from terrestrial laser scanning data. *ISPRS Journal of Photogrammetry and Remote Sensing*, 64(6), 575-584.

[3] Becker, S., & Haala, N. (2007). Refinement of building fassades by integrated processing of LIDAR and image data. *International Archives of Photogrammetry, Remote Sensing and Spatial Information Science*, 36, 7-12.

[4] Binda, L., Lenzi, G., & Saisi, A. (1998). NDE of masonry structures: use of radar tests for the characterisation of stone masonries. *NDT & E International*, 31(6), 411-419.

[5] Brancaccio, A., Soldovieri, F., Leone, G., Sglavo, D., & Pierri, R. (2006). Microwave characterization of materials in civil engineering. *Proceedings of the European Microwave Association,*128, 135.

[6] Fischler, M.A. and Bolles, R.C. (1981). Random sample consensus: a paradigm for model fitting with applications to image analysis and automated cartography. *Commun. ACM,* 24 (6), 381-395.

[7] Bogdan Rusu, R. (2009). Semantic 3D Object Maps for Everyday Manipulation in Human Living Environments. PhD Thesis. Computer Science department, Technische Universitaet Muenchen, Germany.

[8] Soumekh, M. (1999). *Synthetic aperture radar signal processing* (Vol. 7). New York: Wiley.